Operating regimes for single and multiple wireless power transfer links

Mauro Mongiardo

Department of Engineering, University of Perugia, Italy

Table of contents

Measurement of WPT links

WPT: Measurement

- We need a measurement methodology to accurately characterize WPT links, i.e. to estimate the power transfer performance, the link efficiency, and the links characteristics while the system is operational.

WPT: Measurement

- We need a measurement methodology to accurately characterize WPT links, i.e. to estimate the power transfer performance, the link efficiency, and the links characteristics while the system is operational.

- Measurement technique depends on the selected frequency range

WPT: Measurement

- We need a measurement methodology to accurately characterize WPT links, i.e. to estimate the power transfer performance, the link efficiency, and the links characteristics while the system is operational.
- Measurement technique depends on the selected frequency range
- Lower frequency measurement technique (operational amplifier).

WPT: Measurement

- We need a measurement methodology to accurately characterize WPT links, i.e. to estimate the power transfer performance, the link efficiency, and the links characteristics while the system is operational.
- Measurement technique depends on the selected frequency range
- Lower frequency measurement technique (operational amplifier).
- Higher frequency measurement technique via vectorial network analyzer (VNA).

- We need a measurement methodology to accurately characterize WPT links, i.e. to estimate the power transfer performance, the link efficiency, and the links characteristics while the system is operational.
- Measurement technique depends on the selected frequency range
- Lower frequency measurement technique (operational amplifier).
- Higher frequency measurement technique via vectorial network analyzer (VNA).
- Warning: when trying to measure highly resonant structures using reference impedances may prevent accuracy.

Example of a measurement case at low frequency of two synchronous resonators (tuned to the same nominal resonant frequency).
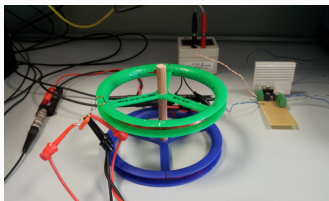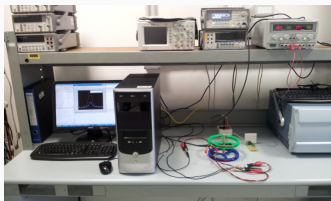

Figure 1: Picture of the experimental setup (a), and magnification of the WPT link (b). The realized air-core inductors are shown on the bench in (b), with the primary on the bottom and the secondary on the top at a distance of 75 mm. The realized unity-gain buffer circuit is shown on the right side in (b).
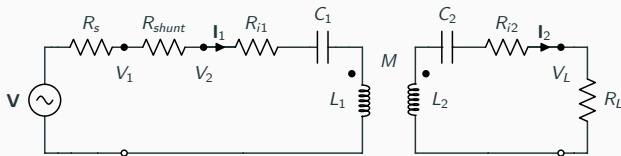
Figure 2: Considered WPT circuit, showing the nodes where the voltages V_1, V_2, and V_L are measured, denoted as black dots.
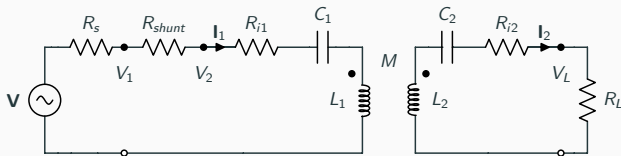
Figure 2: Considered WPT circuit, showing the nodes where the voltages V_1, V_2, and V_L are measured, denoted as black dots.
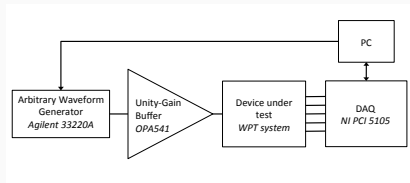
Figure 3: Block diagram of the experimental setup.

WPT: Measurement

The mutual coupling between the primary and secondary circuit is modeled by the mutual inductance $M = k\sqrt{L_1 L_2}$, with k being the coupling coefficient. We have:

$$\begin{cases} I_1 \left(R_s + R_{i1} - j\frac{1}{\omega C_1} + j\omega L_1 \right) - j\omega M I_2 = V \\ -j\omega M I_1 + I_2 \left(R_L + R_{i2} - j\frac{1}{\omega C_2} + j\omega L_2 \right) = 0 \,. \end{cases} \tag{1}$$

WPT: Measurement

The mutual coupling between the primary and secondary circuit is modeled by the mutual inductance $M = k\sqrt{L_1 L_2}$, with k being the coupling coefficient. We have:

$$\begin{cases} I_1 \left(R_s + R_{i1} - j\frac{1}{\omega C_1} + j\omega L_1 \right) - j\omega M I_2 = V \\ -j\omega M I_1 + I_2 \left(R_L + R_{i2} - j\frac{1}{\omega C_2} + j\omega L_2 \right) = 0 \,. \end{cases} \quad (1)$$

Assume $Z_{Loop1} = R_s + R_{i1} - j\frac{1}{\omega C_1} + j\omega L_1$ and $Z_{Loop2} = R_L + R_{i2} - j\frac{1}{\omega C_2} + j\omega L_2$:

$$\begin{cases} I_1 Z_{Loop1} - j\omega M I_2 = V \\ -j\omega M I_1 + I_2 Z_{Loop2} = 0 \,. \end{cases} \quad (2)$$

WPT: Measurement

The solution of (2) provides the following expressions for the currents at the primary and secondary coils:

$$I_1 = V \left(\frac{Z_{Loop2}}{Z_{Loop1} Z_{Loop2} + \omega^2 M^2} \right) \tag{3}$$

$$I_2 = j\omega M V \left(\frac{1}{Z_{Loop1} Z_{Loop2} + \omega^2 M^2} \right) \tag{4}$$

Once the source voltage V and the load impedance R_L are known, it is possible to derive a procedure for the characterization of the mutual inductance of the WPT link. For the case when the receiving coil is at given distance from the transmitting coil, the procedure can be summarized by the following steps:

WPT: Measurement

Step 1: Perform a measurement of the Z_{Loop1} without the coupling with the secondary coil;

WPT: Measurement

Step 1: Perform a measurement of the Z_{Loop1} without the
coupling with the secondary coil;

Step 2: Perform a measurement of the Z_{in} for a given distance
between the primary coil and secondary coil;

$$Z_{in} = \frac{V}{I_1} = Z_{Loop1} + \frac{\omega^2 M^2}{Z_{Loop2}} \tag{5}$$

WPT: Measurement

Step 1: Perform a measurement of the Z_{Loop1} without the coupling with the secondary coil;

Step 2: Perform a measurement of the Z_{in} for a given distance between the primary coil and secondary coil;

$$Z_{in} = \frac{V}{I_1} = Z_{Loop1} + \frac{\omega^2 M^2}{Z_{Loop2}} \tag{5}$$

Step 3: Perform a measurement of the I_2 for a given distance on a known load Z_L;

Step 1: Perform a measurement of the Z_{Loop1} without the coupling with the secondary coil;

Step 2: Perform a measurement of the Z_{in} for a given distance between the primary coil and secondary coil;

$$Z_{in} = \frac{V}{I_1} = Z_{Loop1} + \frac{\omega^2 M^2}{Z_{Loop2}} \tag{5}$$

Step 3: Perform a measurement of the I_2 for a given distance on a known load Z_L;

Step 4: Compute the following quantities:

$$\beta = Z_{in} - Z_{Loop1} = \frac{\omega^2 M^2}{Z_{Loop2}} \tag{6}$$

$$\gamma = I_2 \frac{1}{\beta} = j\frac{V}{\omega M}\left(\frac{Z_{Loop2}}{Z_{Loop1}Z_{Loop2} + \omega^2 M^2}\right) = j\frac{I_1}{\omega M} \tag{7}$$

$$M = j\frac{I_1}{\omega \gamma}. \tag{8}$$

WPT: Measurement

Voltage signals at the three considered nodes in the circuit are digitized using a data acquisition board, NI PCI 5105 by National Instruments. In particular, five simultaneous channels sampling at 1 MSa/s, 12 bits, with a range of 6 V are used. Sinusoidal signals of 0.5Vpp at a set of frequencies spanning the [15 kHz 35 kHz] interval at 500 Hz steps are generated, and a 10 ms record is acquired for each frequency.

The OPA541 power operational amplifier was used in a voltage follower configuration to implement a unity-gain voltage buffer.

WPT: Measurement

Two resonators tuned to the same nominal resonant frequency of 24.48 kHz were employed. The resonators are implemented by means of 330 nF nominal–value capacitors and 128 µH nominal–value inductors, which are air-core copper wire coils of diameter 140 mm and number of turns equal to 20.

WPT: Measurement

Two resonators tuned to the same nominal resonant frequency of 24.48 kHz were employed. The resonators are implemented by means of 330 nF nominal–value capacitors and 128 µH nominal–value inductors, which are air-core copper wire coils of diameter 140 mm and number of turns equal to 20.

The current in the primary is measured by using a shunt resistor of nominal value $R_{shunt} = 1\,\Omega$. Furthermore, the load is realized by a resistor of nominal value $R_L = 5\,\Omega$. Both the shunt resistor and the load resistor are measured in the initial calibration phase using a multimeter.

WPT: Measurement

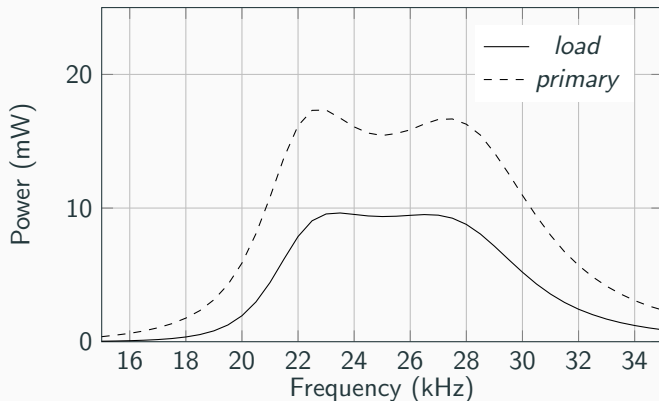Measured active power. Two separate resonances are clearly visible.

Figure 4: Experimental behavior of power vs frequency with coils placed at a distance of 33 mm. Active power on the load (solid line) and power in the primary (dotted line).
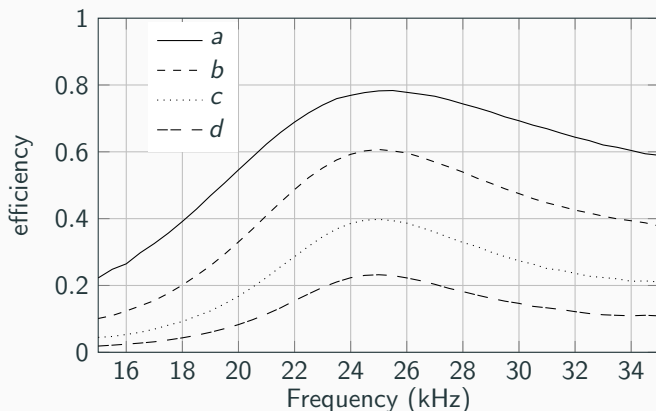
Figure 5: Power transfer efficiency vs frequency with coils placed at different distances. a: 16 mm; b: 33 mm; c: 54 mm; d: 75 mm.
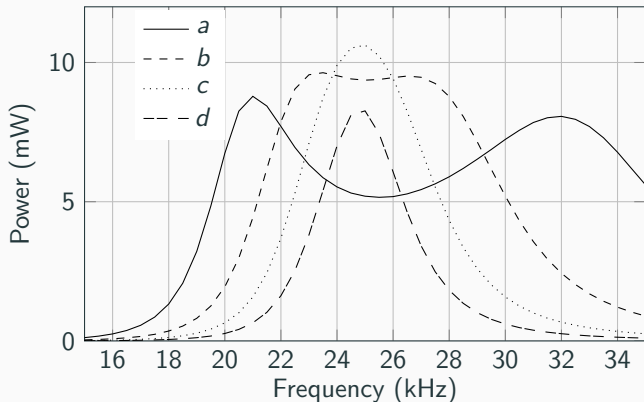
Figure 6: Power at the load for different distances. a: 16 mm; b: 33 mm; c: 54 mm; d: 75 mm.

When increasing the coupling the power on the load diminishes.

Is it possible to find a remedy to this situation?

When increasing the coupling the power on the load diminishes.

Is it possible to find a remedy to this situation?

One possible operating regime is to keep the frequency fixed and to change the load value.

When increasing the coupling the power on the load diminishes.

Is it possible to find a remedy to this situation?

One possible operating regime is to keep the frequency fixed and to change the load value.

Another operating regime will be discussed next in the part of the presentation referring to coupling–independent WPT.

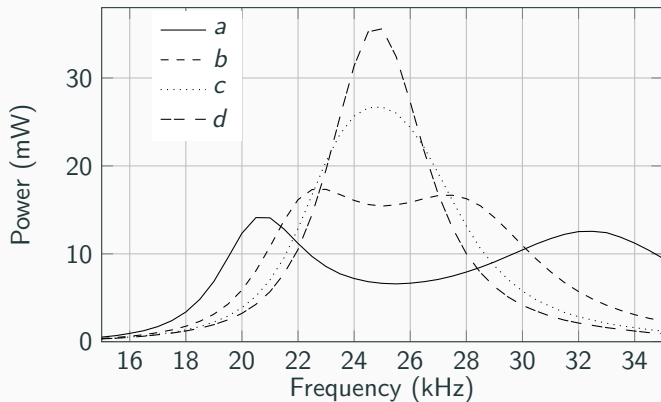**Figure 7:** Active power at the primary for different distances. a: 16 mm; b: 33 mm; c: 54 mm; d: 75 mm.

WPT: Measurement of impedance

In strong-coupling conditions, the input impedance of the WPT system is purely real at three frequencies, corresponding to the resonances.
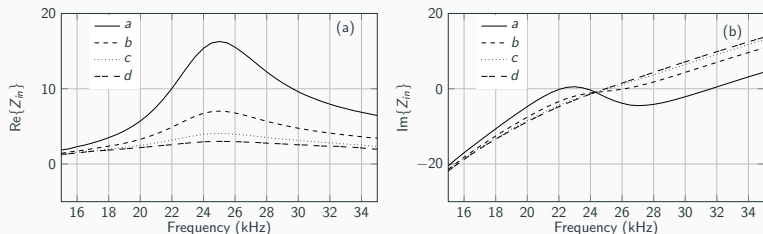

Figure 8: Measured input impedance, real (a) and imaginary (b) part, at different distances. a: 16 mm; b: 33 mm; c: 54 mm; d: 75 mm.

WPT: Measurement

The estimated values of M at several distances between the centers of the coils are listed in Table 1, and compared with measurement results. The latter were obtained off–line by disconnecting the measurement system, the source generator and the load from the WPT and using a LCR meter.

The estimated and measured values show a discrepancy that is below 9% at all considered distances. Such discrepancy can be attributed to uncertainties in the coil alignment and distance measurement.

Table 1: Estimated and measured values of mutual inductance at different distances.

case	a	b	c	d
distance (mm)	16	33	54	75
estimated M (µH)	53.4	36.2	22.6	14.6
measured M (µH)	55.8	34.1	20.6	13.3
relative deviation (%)	4.5	5.8	8.8	8.9

It is possible to show that the following results hold true:

Table 2: A summary of the parameters values for the approaches that maximize efficiency and power transferred to the load. The parameters have the following meanings: $\chi = (\omega M)/\sqrt{r_{11} r_{22}}$, $\theta = \sqrt{1 + \chi^2}$, $r_{11} = R_s + R_{i1}$, $r_{22} = R_{i2}$. The power has been normalized to $P_0 = V^2/(8r_{11})$.

Parameter	maximum efficiency	maximum power
R_L	$r_{22}\theta$	$r_{22}\theta^2$
R_{in}	$r_{11}\theta$	$2r_{11}\theta^2/(1 + \theta^2)$
P_{in}	$4/\theta$	$2(1 + \theta^2)/\theta^2$
P_L	$4\eta_1/\theta$	χ^2/θ^2
η	$\eta_1 = \chi^2/(1 + \theta)^2$	$\chi^2/(2(1 + \theta^2))$

WPT: Measurement

According to the terminology of Table 2 we have:

$$
\begin{aligned}
r_{11} &= R_s + R_{i1} = 0.83\,\Omega \\
r_{22} &= R_{i2} = 0.84\,\Omega \\
M &= 34.1\,\mu H \\
\omega &= 2\pi f, \text{with } f = 24.610\,kHz \\
\chi &= \frac{\omega M}{\sqrt{r_{11} r_{22}}} = 6.33 \\
\theta &= \sqrt{1 + \chi^2} = 6.421\,.
\end{aligned} \tag{9}
$$

WPT: Measurement

The performance of the system has been computed for the maximum efficiency and maximum power operation and the results are given in Table 3. It is worth to note that the experiment has been performed using a different load resistance. Nevertheless, the slight difference has led to similar values of the measured efficiency and of the theoretical one. The maximum power operation case has not been measured.

Table 3: Parameterization for maximum efficiency and maximum power of the considered test case WPT link.

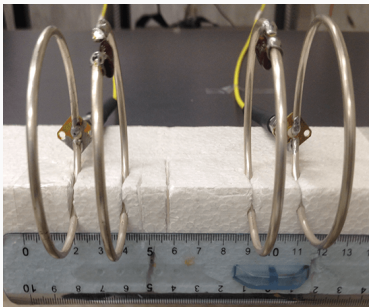| Parameter	maximum efficiency	maximum power
R_L (Ω)	5.386	34.53
R_{in} (Ω)	5.322	1.621
P_{in} (mW)	4.97	16
P_L (mW)	3.629	7.77
η	.73	0.476

Figure 9: Experimental realization of a WPT system composed by a four-coil structure; the first and last coils (input/output) are inductively coupled with the second and third coils, which are resonant and which perform the sought wireless power transmission.
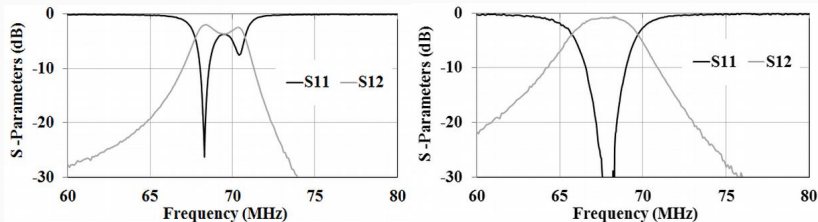
Figure 10: Measured scattering parameters of the WPT system. Left: reference impedance on 50 Ω. Right: using as reference the conjugate image impedances.
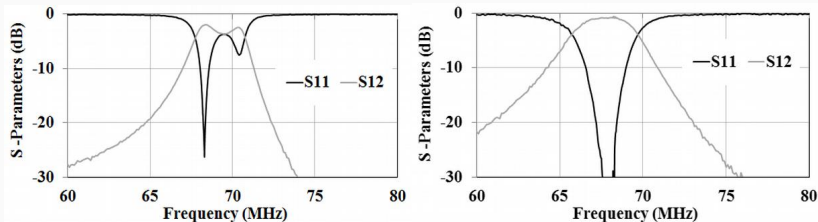
Figure 10: Measured scattering parameters of the WPT system. Left: reference impedance on 50 Ω. Right: using as reference the conjugate image impedances.

Standard reference impedances does not work!

From **S** matrix pass to **Z** matrix and compute the conjugate image impedances.
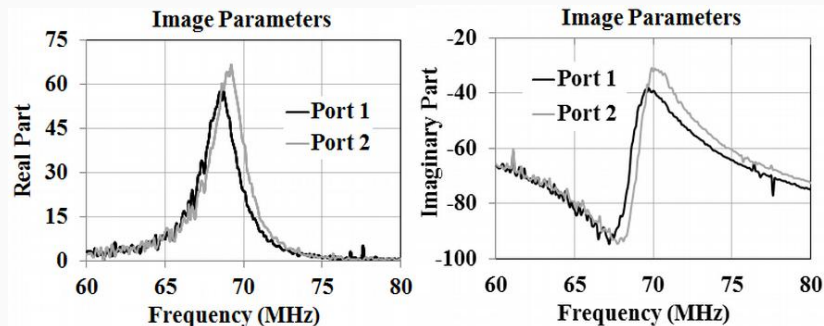
Figure 11: Conjugate image impedances of the WPT system.

WPT: Measurement

For example, consider, at the frequency of 68 MHz, the measured scattering matrix is:

$$\mathbf{S} = \begin{pmatrix} 16.4641 + j9.8042 & 12.3951 - j79.1614 \\ 12.3951 - j79.1614 & 13.2239 + j32.3103 \end{pmatrix}. \tag{10}$$

The relative conjugate image impedances are $Z_{c1} = 47.5414 - j84.799$ and $Z_{c2} = 38.1850 - j92.5459$.

We need to to insert two capacitors $C_1 = 27.6\,\text{pF}$ and $C_2 = 25.3\,\text{pF}$ at port 1 and 2, respectively.

The normalization impedances are now $Z_1 = 47.5\,\Omega$ and $Z_2 = 38.2\,\Omega$.

Note that Conjugate Image Impedances are different from standard Image Impedances. As an example, the image impedances for the previous example are $Z_{i1} = 59.6589 + j6.9209$ and $Z_{i2} = 94.4249 - j55.2906$.

What are the conjugate image impedances?

And how to compute them?

This will be the topic of a next part of the presentation.

Conjugate Image Impedances

Figure 12: Conjugate Image Impedances Definition.

The conjugate-image impedances can be expressed in terms e.g. of the impedance network parameters.

$$v_1 = z_{11} i_1 + z_{12} i_2 \qquad (11)$$

$$v_2 = z_{21} i_1 + z_{22} i_2 \qquad (12)$$

Assuming $z_{ij} = r_{ij} + j x_{ij}$ with $i, j = 1, 2$ the conjugate–image impedances are given by:

$$Z_{c1} = r_{11}(\theta_r + j\theta_x) - jx_{11} \qquad (13)$$

$$Z_{c2} = r_{22}(\theta_r + j\theta_x) - jx_{22} \qquad (14)$$

By introducing the following variables:

$$\sqrt{z_{12}z_{21}} = r_c + jx_c, \tag{15}$$

we obtain the solutions for θ_r and θ_x as:

$$\theta_r = \sqrt{\left(1 - \frac{r_c^2}{r_{11}r_{22}}\right)\left(1 + \frac{x_c^2}{r_{11}r_{22}}\right)} \tag{16}$$

$$\theta_x = \frac{r_c x_c}{r_{11}r_{22}} \tag{17}$$

When the two port networks considered for wireless power transfer are reciprocal, i.e. $z_{12} = z_{21}$, the following simplification occurs:

$$\theta_r = \sqrt{\left(1 - \frac{r_{12}^2}{r_{11}r_{22}}\right)\left(1 + \frac{x_{12}^2}{r_{11}r_{22}}\right)} \tag{18}$$

$$\theta_x = \frac{r_{12} x_{12}}{r_{11}r_{22}} \tag{19}$$

Roberts has introduced the conjugate image impedances in 1946. here we present a different method for their computation.

With reference to Fig. 12, the conjugate image impedances can be calculated from the impedance coefficients of the network with the appropriate terminating impedances. If we let $v_2 = -i_2 Z_{c2}$ in eq. (12) and solve eq. (11) for v_1/i_1, we get the reflected impedances

$$Z_{c1}^* = z_{11} - \frac{z_{12}z_{21}}{z_{22} + Z_{c2}};$$

(20)

in a similar way we have:

$$Z_{c2}^* = z_{22} - \frac{z_{12}z_{21}}{z_{11} + Z_{c1}}.$$

(21)

Conjugate Image impedances: computation 2

Let us now take the complex conjugate of eq. (21) which gives:

$$Z_{c2} = z_{22}^* - \frac{z_{12}^* z_{21}^*}{z_{11}^* + Z_{c1}^*}. \tag{22}$$

By substituting eq. (22) into eq. (20)

$$Z_{c1}^* = z_{11} - \frac{z_{12} z_{21}}{z_{22} + z_{22}^* - \frac{z_{12}^* z_{21}^*}{z_{11}^* + Z_{c1}^*}}; \tag{23}$$

or equivalently

$$Z_{c1}^* - z_{11} = -\frac{z_{12} z_{21}(z_{11}^* + Z_{c1}^*)}{(z_{22} + z_{22}^*)(z_{11}^* + Z_{c1}^*) - z_{12}^* z_{21}^*}. \tag{24}$$

Conjugate Image impedances: computation 3

Note that $z_{22} + z_{22}^* = 2r_{22}$ and $z_{11} + z_{11}^* = 2r_{11}$; introduce:

$$\xi = z_{11}^* + Z_{c1}^*; \tag{25}$$

which, inserted in eq. (24), provides:

$$(\xi - 2r_{11})[2r_{22}\xi - z_{12}^* z_{21}^*] + z_{12}z_{21}\xi = 0. \tag{26}$$

By setting:

$$
\begin{align}
a &= 2r_{22} \tag{27}\\
b &= -4(r_{11}r_{22} - jr_{12}x_{12}) \tag{28}\\
c &= 2r_{11}\left[r_{12}^2 - x_{12}^2 - 2jr_{12}x_{12}\right] \tag{29}
\end{align}
$$

we obtain the second order equation

$$a\xi^2 + b\xi + c = 0. \tag{30}$$

The solution with positive real part provides, via eq. (25), the sought conjugate image impedance Z_{c1}^*; from the latter, by using eq. (22) the value of Z_{c2} is also recovered.

33

Conjugate Image Impedance: equivalence

The conjugate image impedances are also the impedances that realize maximum efficiency.

Parameter	maximum efficiency	maximum power	conjugate matching
R_L	$r_{22}\theta_r$	$r_{22}\theta_r^2/(\theta_x^2+1)$	$r_{22}\theta_r$
X_L	$r_{22}\theta_x - x_{22}$	$-x_{22} + r_{22}\theta_x + r_{22}\theta_x\theta_r^2/(\theta_x^2+1)$	$r_{22}\theta_x - x_{22}$
R_{c1}	0	0	$r_{11}\theta_r$
X_{c1}	$x_{12}r_{12}/r_{22} - x_{11}$	$x_{12}r_{12}/r_{22} - x_{11}$	$x_{12}r_{12}/r_{22} - x_{11}$
R_{in}	$r_{11}\theta_r$	$2r_{11}\theta_r^2/(1+\theta_r^2+\theta_x^2)$	$2r_{11}\theta_r$
X_{in}	0	0	0
P_{in}	$4/\theta_r$	$2(1+\theta_r^2+\theta_x^2)/(\theta_r^2)$	$2/(\theta_r)$
P_L	$4\eta_1/\theta_r$	$(\xi^2+\chi^2)/(\theta_r^2)$	$2\eta_1/(\theta_r)$
η	$\eta_1 = (\xi^2+\chi^2)/((1+\theta_r)^2+\theta_x^2)$	$(\xi^2+\chi^2)/(2(1+\theta_r^2+\theta_x^2))$	$\eta_1/2$

Table 4: A summary of the parameters values for the approaches that maximize efficiency, power and conjugate matching. The parameters have the following meanings: $\chi = x_{12}/\sqrt{r_{11}r_{22}}$, $\xi = r_{12}/\sqrt{r_{11}r_{22}}$, $\theta_r = \sqrt{1+\chi^2}\sqrt{1-\xi^2}$, $\theta_x = \chi\xi$. Powers have been normalized to $P_0 = V_1^2/(8r_{11})$.

Conjugate Image Impedance: A word of caution!
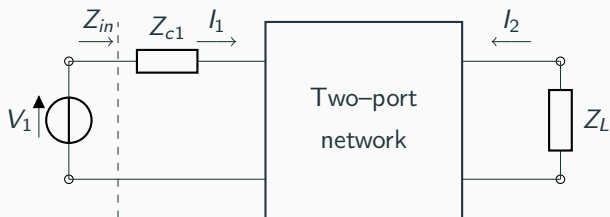
Figure 13: Two–port network with added impedance $Z_{c1} = R_{c1} + jX_{c1}$. The value of X_{c1} is given in table (4), while $R_{c1} = 0$ for both the maximum efficiency and maximum power transfer approach. For conjugate matching the value of Z_{c1} is given in table (4).

Coupling–Independent Wireless Power Transfer for Series Resonators

Frequency agile WPT

- Mid–range wireless power transfer can be achieved e.g. by
  employing mutually coupled resonant circuits.

Frequency agile WPT

- Mid–range wireless power transfer can be achieved e.g. by employing mutually coupled resonant circuits.
- When operating at the resonant frequency, the loads that realizes maximum power transfer or maximum efficiency are *coupling–dependent*.

- Mid–range wireless power transfer can be achieved e.g. by employing mutually coupled resonant circuits.

- When operating at the resonant frequency, the loads that realizes maximum power transfer or maximum efficiency are *coupling–dependent*.

- **An alternative operating regime**

  By selecting a suitable frequency, it is feasible, after a certain threshold value of the coupling, to obtain *coupling–independent* wireless power transfer.

- Maximum Power Transfer Efficiency (MPTE) can be realized by using conjugate image impedances.

- Maximum Power Transfer Efficiency (MPTE) can be realized by using conjugate image impedances.
- For a given value of the coupling, we can select the load in such a way to achieve either Maximum Power Delivered to the Load (MPDL) or MPTE.

- Maximum Power Transfer Efficiency (MPTE) can be realized by using conjugate image impedances.
- For a given value of the coupling, we can select the load in such a way to achieve either Maximum Power Delivered to the Load (MPDL) or MPTE.
- In both cases the operating frequency is the resonant one and the load values are coupling dependent.

- Maximum Power Transfer Efficiency (MPTE) can be realized by using conjugate image impedances.
- For a given value of the coupling, we can select the load in such a way to achieve either Maximum Power Delivered to the Load (MPDL) or MPTE.
- In both cases the operating frequency is the resonant one and the load values are coupling dependent.
- With MPDL/MPTE solutions there is no frequency splitting phenomena.

- When a fixed load value is used there is an optimal coupling and either "over–coupled" or "under–coupled" solutions as the coupling is varied.

- When a fixed load value is used there is an optimal coupling and either "over–coupled" or "under–coupled" solutions as the coupling is varied.

- "over–coupled": frequency splitting which is manifested by the presence of two peaks of the power on the load at two frequencies different from the resonant one.

- When a fixed load value is used there is an optimal coupling and either "over–coupled" or "under–coupled" solutions as the coupling is varied.

- "over–coupled": frequency splitting which is manifested by the presence of two peaks of the power on the load at two frequencies different from the resonant one.

- once the coupling is greater than a threshold value, in addition to the main resonant frequency, also two other frequencies exist for which the input impedance is purely resistive.

Frequency agile WPT: frequency splitting

- When a fixed load value is used there is an optimal coupling and either "over–coupled" or "under–coupled" solutions as the coupling is varied.

- "over–coupled": frequency splitting which is manifested by the presence of two peaks of the power on the load at two frequencies different from the resonant one.

- once the coupling is greater than a threshold value, in addition to the main resonant frequency, also two other frequencies exist for which the input impedance is purely resistive.

- At these operating frequencies the load resistance is reproduced, apart for a fixed scaling factor, at the input port, independently of the coupling. We thus achieve a coupling–independent operating regime.

Schematic of the WPT link realized with compensated coupled inductors
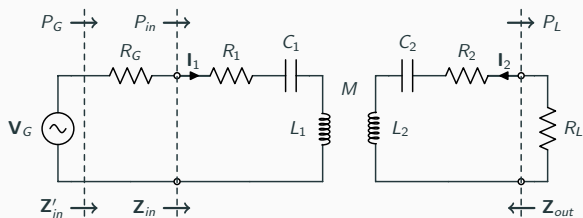
Figure 14: Schematic of the WPT link.

- In Fig. 14 we have a WPT link realized by two coupled series resonators, driven by a sinusoidal voltage generator $v_G(t) = \sqrt{2}\,V_G \cos(\omega t)$, with internal resistance R_G and connected to a resistive load R_L.

- The resistors R_1 and R_2 represent the resonator losses.

- We assume that the resonators are synchronous (same free resonant angular frequency $\omega_0 = 1/\sqrt{L_1 C_1} = 1/\sqrt{L_2 C_2}$).

- In Fig. 14 we have a WPT link realized by two coupled series resonators, driven by a sinusoidal voltage generator $v_G(t) = \sqrt{2}\, V_G \cos(\omega t)$, with internal resistance R_G and connected to a resistive load R_L.

- The resistors R_1 and R_2 represent the resonator losses.

- We assume that the resonators are synchronous (same free resonant angular frequency $\omega_0 = 1/\sqrt{L_1 C_1} = 1/\sqrt{L_2 C_2}$).

- The coupled inductors can be represented by the equivalent circuit of Fig. 15, where $k = M/\sqrt{L_1 L_2}$ is the coupling coefficient and the transform ratio is $n = \sqrt{L_1/L_2}$.

- In Fig. 14 we have a WPT link realized by two coupled series resonators, driven by a sinusoidal voltage generator $v_G(t) = \sqrt{2}\, V_G \cos(\omega t)$, with internal resistance R_G and connected to a resistive load R_L.

- The resistors R_1 and R_2 represent the resonator losses.

- We assume that the resonators are synchronous (same free resonant angular frequency $\omega_0 = 1/\sqrt{L_1 C_1} = 1/\sqrt{L_2 C_2}$).

- The coupled inductors can be represented by the equivalent circuit of Fig. 15, where $k = M/\sqrt{L_1 L_2}$ is the coupling coefficient and the transform ratio is $n = \sqrt{L_1/L_2}$.

- Hence, by referring the parameters of the secondary side to the primary, we obtain the equivalent circuit of Fig. 16, which contains two resonators with identical inductances and capacitances.

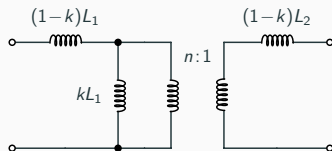# Equivalent circuit of the WPT link referred to primary

Figure 15: Equivalent circuit of two coupled inductors.
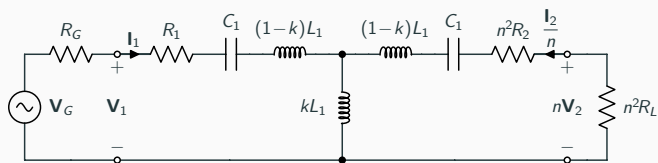

Figure 16: Equivalent circuit of the WPT link referred to primary.

Normalization

We define the *normalized frequency* $u = \omega/\omega_0$ and the *reactance slope parameter* of the primary resonator $X_0 = \sqrt{L_1/C_1}$ which also represents the common (absolute) value of the reactances of the primary inductor and capacitor at $\omega = \omega_0$.

Normalize the impedances of the circuit of Fig. 16 with respect to X_0.

The *normalized resistances* are reported in table 5.

Table 5: Normalized resistances

$$r_1 = R_1/X_0 = 1/Q_1 \qquad r_2 = n^2 R_2/X_0 = 1/Q_2$$
$$r_G = R_G/X_0 = 1/Q_G \qquad r_L = n^2 R_L/X_0 = 1/Q_L$$
$$r_{1T} = r_1 + r_G = 1/Q_{1T} \qquad r_{2T} = r_2 + r_L = 1/Q_{2T}$$

Note that r_1, r_G and r_{1T} are the reciprocal of the unloaded, external and loaded quality factor of the primary resonator, respectively, and that r_2, r_L and r_{2T} have an analogous meaning for the secondary resonator.

INPUT IMPEDANCE COMPUTATION

Let us start by considering the ABCD matrix of coupled LCs (see Fig. 16). For the normalized series reactive elements we have:

$$T_1 = \begin{pmatrix} 1 & -\dfrac{j\left((k-1)\,u^2+1\right)}{u} \\ 0 & 1 \end{pmatrix} \tag{31}$$

INPUT IMPEDANCE COMPUTATION

Let us start by considering the ABCD matrix of coupled LCs (see Fig. 16). For the normalized series reactive elements we have:

$$T_1 = \begin{pmatrix} 1 & -\frac{j\left((k-1)\,u^2+1\right)}{u} \\ 0 & 1 \end{pmatrix} \tag{31}$$

while the normalized shunt element is

$$T_2 = \begin{pmatrix} 1 & 0 \\ -\frac{j}{k\,u} & 1 \end{pmatrix} \tag{32}$$

INPUT IMPEDANCE COMPUTATION

Let us start by considering the ABCD matrix of coupled LCs (see Fig. 16). For the normalized series reactive elements we have:

$$T_1 = \begin{pmatrix} 1 & -\frac{j\left((k-1)u^2+1\right)}{u} \\ 0 & 1 \end{pmatrix} \tag{31}$$

while the normalized shunt element is

$$T_2 = \begin{pmatrix} 1 & 0 \\ -\frac{j}{ku} & 1 \end{pmatrix} \tag{32}$$

giving the total ABCD matrix as

$$
\begin{aligned}
T_1 T_2 T_1 &\doteq \begin{pmatrix} A & B \\ C & D \end{pmatrix} \\
&= \begin{pmatrix} \frac{u^2-1}{ku^2} & -\frac{j\left((k^2-1)u^4+2u^2-1\right)}{ku^3} \\ -\frac{j}{ku} & \frac{u^2-1}{ku^2} \end{pmatrix}
\end{aligned} \tag{33}
$$

As well known, the latter when evaluated at $u = 1$ becomes an immittance inverter.

Input Impedance

Now we investigate the behavior of the input impedance z_{in}, with respect to the normalized frequency u, for a given terminating impedance r_{2T}; in terms of the ABCD parameters we have:

$$
\begin{aligned}
z_{in} &= r_{in} + jx_{in} = r_1 + \frac{Ar_{2T} + B}{Cr_{2T} + D} \qquad (34) \\
r_{in} &= r_1 + \frac{k^2\, u^4\, r_{2T}}{u^4 - (2 - r_{2T}^2)\, u^2 + 1} \\
x_{in} &= \frac{(u^2 - 1)\left[(1 - k^2)\, u^4 - (2 - r_{2T}^2)\, u^2 + 1\right]}{u\left[u^4 - (2 - r_{2T}^2)\, u^2 + 1\right]}.
\end{aligned}
$$

Main and secondary resonant frequencies

From (34) the input reactance vanish at $u_0 = 1$, (*main resonant frequency*).

The input impedance exhibits two *secondary resonant frequencies* (frequency bifurcation) when the equation

$$\left(1 - k^2\right) x^2 - \left(2 - r_{2T}^2\right) x + 1 = 0, \tag{35}$$

with $x = u^2$, admits two real positive solutions.

Main and secondary resonant frequencies

From (34) the input reactance vanish at $u_0 = 1$, (*main resonant frequency*).

The input impedance exhibits two *secondary resonant frequencies* (frequency bifurcation) when the equation

$$\left(1 - k^2\right) x^2 - \left(2 - r_{2T}^2\right) x + 1 = 0, \tag{35}$$

with $x = u^2$, admits two real positive solutions.

Making use of Descartes' sign rule and requiring that the discriminant of (35) is nonnegative, we obtain that these additional resonances exist if

$$r_{2T} < \sqrt{2} \tag{36}$$

$$k \geq k_b = r_{2T} \sqrt{1 - \frac{r_{2T}^2}{4}} \tag{37}$$

where k_b represents the value of the coupling factor at which frequency bifurcation occurs.

Main and secondary resonant frequencies

From (34) the input reactance vanish at $u_0 = 1$, (*main resonant frequency*).

The input impedance exhibits two *secondary resonant frequencies* (frequency bifurcation) when the equation

$$\left(1 - k^2\right) x^2 - \left(2 - r_{2T}^2\right) x + 1 = 0, \tag{35}$$

with $x = u^2$, admits two real positive solutions.

Making use of Descartes' sign rule and requiring that the discriminant of (35) is nonnegative, we obtain that these additional resonances exist if

$$r_{2T} < \sqrt{2} \tag{36}$$

$$k \geq k_b = r_{2T} \sqrt{1 - \frac{r_{2T}^2}{4}} \tag{37}$$

where k_b represents the value of the coupling factor at which frequency bifurcation occurs.

In practical cases $k_b \approx r_{2T}$.

When (36) and (37) hold, the input reactance also vanishes at

$$u_{\pm} = \sqrt{\frac{2 - r_{2T}^2 \pm \sqrt{4k^2 + r_{2T}^4 - 4r_{2T}^2}}{2(1 - k^2)}} \qquad (38)$$

Secondary Resonant Frequencies

When (36) and (37) hold, the input reactance also vanishes at

$$u_{\pm} = \sqrt{\frac{2 - r_{2T}^2 \pm \sqrt{4k^2 + r_{2T}^4 - 4r_{2T}^2}}{2(1 - k^2)}} \tag{38}$$

From (36)–(38) the secondary resonant frequencies are only determined by k, r_{2T}.

coupling–independent WPT

At $u = u_{\pm}$ the normalized input resistance, for all values of k is

$$r_{in} = r_1 + r_{2T} \tag{39}$$

which corresponds to the unnormalized input resistance

$$R_{in} = R_1 + n^2(R_2 + R_L). \tag{40}$$

At $u = u_{\pm}$ the normalized input resistance, for all values of k is

$$r_{in} = r_1 + r_{2T} \tag{39}$$

which corresponds to the unnormalized input resistance

$$R_{in} = R_1 + n^2(R_2 + R_L). \tag{40}$$

This shows that the coupled resonators, from the input side, act as an ideal transformer with transform ratio equal to n and independent of k. In these conditions the output power, p_L, and the total efficiency, η, are also independent of k

$$p_L = \frac{r_L}{(r_{1T} + r_{2T})^2} \tag{41}$$
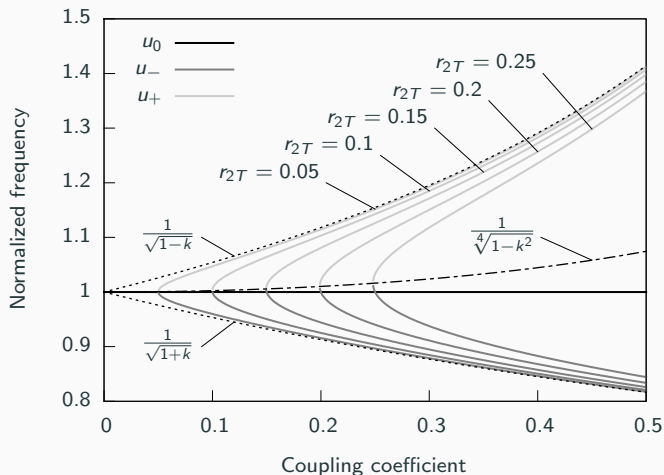
$$\eta = \frac{r_L}{r_{1T} + r_{2T}}. \tag{42}$$

Figure 17: Secondary resonant frequencies behavior as a function of the coupling coefficient.

For $k \gg r_{2T}$, (38) can be approximated as:

$$u_{\pm} \approx 1/\sqrt{1 \mp k}. \tag{43}$$

Results

For $k \gg r_{2T}$, (38) can be approximated as:

$$u_\pm \approx 1/\sqrt{1 \mp k}. \tag{43}$$

The bifurcation points do not lay on the straight line $u = 1$.

For $k = k_b$, u_+ and u_- assume the common value

$$u_b = \sqrt{2/(2 - r_{2T}^2)}, \tag{44}$$

hence, by eliminating r_{2T} from (37) and (44), we obtain that the equation of the locus of the bifurcation points is

$$u = 1/\sqrt[4]{1 - k^2}. \tag{45}$$

Results

Les us consider the case $r_1 = r_2 = 0.01$, corresponding to an unloaded Q-factor of 100 for both resonators, and let us also assume a value of 0.01 for r_G and of 0.15 for r_L.

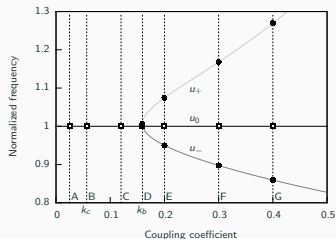In Fig. 18 at $k = k_b$ the bifurcation phenomenon starts.

Figure 18: Main and secondary resonant frequencies as functions of the coupling coefficient.

Results

The various cases are discussed in the following.

1) case A: the output power is lower than the maximum achievable value and its peak is at $u \approx 1$.

Results

The various cases are discussed in the following.

1) case A: the output power is lower than the maximum achievable value and its peak is at $u \approx 1$.

2) case B: corresponds to the critical coupling k_c and the output power is maximum at $u = 1$.

Results

The various cases are discussed in the following.

1) case A: the output power is lower than the maximum achievable value and its peak is at $u \approx 1$.

2) case B: corresponds to the critical coupling k_c and the output power is maximum at $u = 1$.

3) case C: the output power decreases and the power peak splits into two peaks, but still there is no frequency bifurcation.

Results

The various cases are discussed in the following.

1) case A: the output power is lower than the maximum achievable value and its peak is at $u \approx 1$.

2) case B: corresponds to the critical coupling k_c and the output power is maximum at $u = 1$.

3) case C: the output power decreases and the power peak splits into two peaks, but still there is no frequency bifurcation.

4) case D: the frequency bifurcation phenomenon starts.

Results

The various cases are discussed in the following.

1) case A: the output power is lower than the maximum achievable value and its peak is at $u \approx 1$.

2) case B: corresponds to the critical coupling k_c and the output power is maximum at $u = 1$.

3) case C: the output power decreases and the power peak splits into two peaks, but still there is no frequency bifurcation.

4) case D: the frequency bifurcation phenomenon starts.

5) cases E, F, G: for $k > k_b$, when operating at the bifurcated frequencies $u_\pm$ the same output power is obtained, as shown by the flat dotted line. Note that the output power at the resonant frequency $u = 1$ is considerably decreased for these cases. It can also be observed that the curves E, F, G have two additional intersections with the flat line. It is possible to prove that these intersections occur at the frequencies for which the output susceptance vanishes.

Let us consider Figure 19.

The output power reaches its maximum value for $k = k_c = \sqrt{r_{1T} r_{2T}}$, while for $k > k_c$ the output power decreases.

The dashed lines starting at $k = k_b$ correspond to the secondary resonant frequencies $u = u_{\pm}$, which provide constant output power and efficiency as the coupling is increased.

Note that, with respect to the main resonance, at $u = u_{\pm}$ we have a higher output power at the expense of a slightly reduced efficiency.
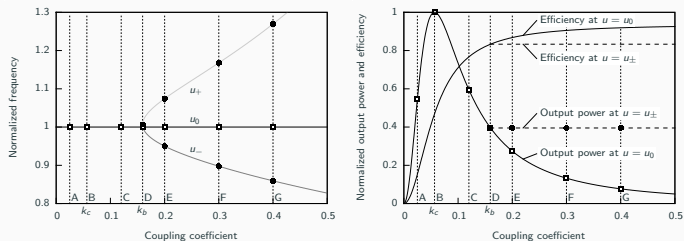
Figure 19: Normalized output power (w.r.t. to its maximum value) and efficiency at the resonant frequencies.

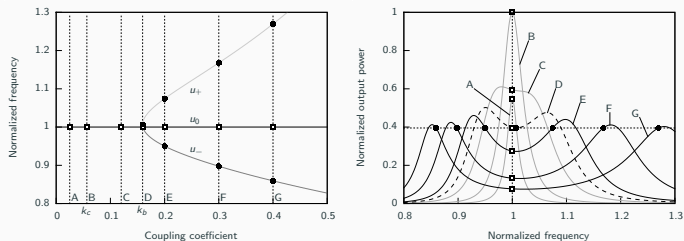**Figure 20:** Normalized output power (w.r.t. its maximum value) for the values of the coupling coefficient at sections A, B, . . ., G in Figs. 18 and 19.

- The problem of measuring wireless power transfer (WPT) links has been considered. Importance of taking into account:
  1. power measurement in addition to scattering parameters;
  2. meaningful normalization i.e. conjugate image impedances

- The problem of measuring wireless power transfer (WPT) links has been considered. Importance of taking into account:
  1. power measurement in addition to scattering parameters;
  2. meaningful normalization i.e. conjugate image impedances
- The conjugate image impedances have been defined and their computation has been described.

Conclusions for two–ports networks

- The problem of measuring wireless power transfer (WPT) links has been considered. Importance of taking into account:
  1. power measurement in addition to scattering parameters;
  2. meaningful normalization i.e. conjugate image impedances
- The conjugate image impedances have been defined and their computation has been described.
- When the load is kept fixed, by operating at a frequency for which we have a zero input reactance , we can achieve coupling–independent WPT.

Three-Ports Networks

Three-Ports Networks

Two different configurations have been investigated.

In one case a single transmitter and two receivers are present.

In the other case two transmitters and a single receiver are employed.

For each case optimal analytical solutions for the load values that maximize power delivered to the load(s) and efficiency have been found and validated by comparisons with circuit simulations.
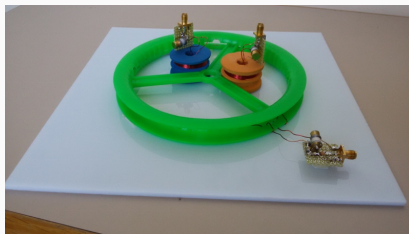

Figure 21: Experiment setup showing three coils resonators.

Introduction

For the case of a single transmitter–single receiver link, the problem of power and efficiency maximization has been analyzed in the literature [2]–[4] and closed form formulas are available.

However, WPT links using either multiple receivers and/or multiple transmitters are of interest [3].

According to the two–port network formalism adopted for a single transmitter–single receiver link, these links can be modeled by using an N–port network where each port is terminated on a transmitter or a receiver.

For multiple receivers and/or transmitters WPT links, some useful results were reported in [5]–[6].

Introduction: state of the art

The problem of efficiency maximization has been solved in [5] for the case of a single transmitter–multiple (uncoupled) receivers link, while in [6] a solution for the case of a two transmitters–single receiver link has been presented.

As for the case of maximizing the power delivered to the load (loads), the solution for a single transmitter–two receivers link has been presented at the APMC 2015 held in Nanjing [7] for the case of uncoupled receivers.

Here the previous analysis is extended to the case of coupled receivers and to the case of a two transmitters–single receiver link.

The general case of non zero mutual couplings between all the three resonators is considered and solved.

For a single transmitter–two receivers link, it is shown that the loads that realize both power and efficiency maximization are purely resistive when the receivers are uncoupled.

It is also demonstrated that the solution for the case when the receivers are coupled is the same as for the uncoupled case except for the presence of appropriate compensating reactances.

For the two transmitters–single receiver configuration, it is demonstrated that the load that realizes power and efficiency maximization is resistive for the case where the transmitters are uncoupled.

In the case when a coupling between the transmitters is present, the optimum load remains purely resistive for efficiency maximization, while a compensating reactance is necessary for power maximization.

For all the analyzed configurations the closed form analytical formulas are derived and validated by comparison with circuit simulation results.

Problem Description

A three-port network consisting of three magnetically coupled LC resonators is considered. The inductance and the capacitance of the i-th resonator are denoted with L_i and C_i, while the mutual inductance between the i-th and the j-th resonator is denoted with $M_{ij} = k_{ij}\sqrt{L_i L_j}$.

It is assumed that the resonators are synchronous: $\omega_0 = \sqrt{C_i L_i}$, $i = 1, 2, 3$. In addition, losses are taken into account by means of equivalent series resistances r_i related to the respective quality factors Q_i by the standard relationships $Q_i = \omega_0 L_i / r_i$, $i = 1, 2, 3$.

At resonance, the following expression can be derived for the impedance matrix of the three-port network:

$$\mathbf{Z} = \begin{pmatrix} r_1 & j\,x_{12} & j\,x_{13} \\ j\,x_{12} & r_2 & j\,x_{23} \\ j\,x_{13} & j\,x_{23} & r_3 \end{pmatrix} \tag{46}$$

where:

$$x_{ij} = \omega M_{ij} \tag{47}$$

Introduction: state of the art

Two different configurations of the network are considered:

- single transmitter–two receivers (1TX-2RX)
- two transmitters–single receiver (2TX-1RX).

Two different solutions of the load impedances are considered:

- the Maximum Power Delivered to the Load (MPDL) solution
  $Z_{Li}^p = R_{Li}^p + jX_{Li}^p$ that maximizes the total active power on the load
  (loads)

$$P_{L,TOT} = \sum P_{L,i} = \sum \frac{1}{2} R_{Li} |I_i|^2 \qquad (48)$$

- the Maximum Power Transfer Efficiency (MPTE) solution
  $Z_{Li}^e = R_{Li}^e + jX_{Li}^e$ that maximizes the efficiency of the link defined as

$$\eta = \frac{P_{L,TOT}}{P_{in,TOT}} = \frac{P_{L,TOT}}{P_{d1} + P_{d2} + P_{d3} + P_{L,TOT}} \qquad (49)$$

where $P_{in,TOT}$ is the total power delivered to the network by the
generators (generator).

One transmitter and two receivers configuration (1TX-2RX)

A voltage generator of amplitude V_1 is placed at port 1, while port 2 and port 3 are terminated on two loads $Z_{Li} = R_{Li} + jX_{Li}$, $i = 2, 3$.

It is convenient to introduce the following parameters

$$\chi_{ij}^2 = \frac{x_{ij}^2}{r_i r_j} \tag{50}$$

and

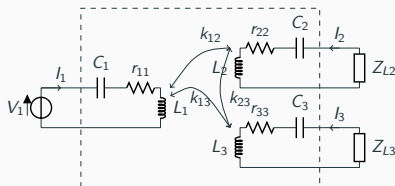$$\theta^2 = 1 + \chi_{12}^2 + \chi_{13}^2. \tag{51}$$

Figure 22: Three–port network showing one transmitter at port 1 and two receivers at port 2 and 3.

1TX–2RX, Uncoupled receivers

For $x_{23} = 0$ both the MPDL and the MPTE solutions are purely resistive (i.e., $Z_{Li}^{p/e} = R_{Li}^{p/e}$) and that the MPDL load is always greater than the MPTE one.

The analytical formulas of the MPTE loads are:

$$
\begin{aligned}
R_{L2}^e &= r_2\theta \\
R_{L3}^e &= r_3\theta.
\end{aligned}
\tag{52}
$$

For the MPDL loads:

$$
\begin{aligned}
R_{L2}^p &= r_2\theta^2 \\
R_{L3}^p &= r_3\theta^2.
\end{aligned}
\tag{53}
$$

with

$$
\theta^2 = 1 + \chi_{12}^2 + \chi_{13}^2.
$$

The general condition for maximum power transfer has been derived in [1] and is expressed by the following relation:

$$\mathbf{I} = (\mathbf{Z_0} + \mathbf{Z_0^*})^{-1}\,\mathbf{E_0} \tag{54}$$

where

$$\mathbf{Z_0} = \begin{pmatrix} \frac{x_{12}^2}{r_1} + r_2 & j\,x_{23} + \frac{x_{12}\,x_{13}}{r_1} \\ j\,x_{23} + \frac{x_{12}\,x_{13}}{r_1} & \frac{x_{13}^2}{r_1} + r_3 \end{pmatrix}. \tag{55}$$

is the impedance matrix of the two-port network obtained when the voltage generator on port one is short–circuited and

$$\mathbf{E_0} = \frac{jV_1}{r_1}\begin{pmatrix} x_{12} \\ x_{13} \end{pmatrix} \tag{56}$$

are Thevenin's equivalent voltage generators on ports two and three. By using (54), the following expression can be derived for the load currents [8]:

$$\mathbf{I} = \frac{jV_1}{2\theta^2}\begin{pmatrix} \frac{x_{12}}{r_1 r_2} \\ \frac{x_{13}}{r_1 r_3} \end{pmatrix}. \tag{57}$$

The corresponding voltages $\mathbf{V}$ are given by $\mathbf{V} = \mathbf{E}_0 - \mathbf{Z}_0(\mathbf{Z}_0 + \mathbf{Z}_0^*)^{-1}\mathbf{E}_0$ as:

$$\mathbf{V} = \frac{V_1}{2}\begin{pmatrix} \frac{x_{13}x_{23}}{\theta^2 r_1 r_3} + j\frac{x_{12}}{r_1} \\ \frac{x_{12}x_{23}}{\theta^2 r_1 r_2} + j\frac{x_{13}}{r_1} \end{pmatrix}. \tag{58}$$

By dividing terms by terms the voltages $\mathbf{V}$ and the currents $\mathbf{I}$ the sought load impedances $Z_{Li} = R_{Li} + jX_{Li}$ with $i = 2, 3$ can be derived:

$$
\begin{aligned}
R_{L2}^p &= r_2\theta^2 \\
X_{L2} &= -\frac{r_2\,x_{13}\,x_{23}}{r_3\,x_{12}} \\
R_{L3}^p &= r_3\theta^2 \\
X_{L3} &= -\frac{r_3\,x_{12}\,x_{23}}{r_2\,x_{13}}.
\end{aligned} \tag{59}
$$

It is possible to shown that these results are also valid for the case of maximum efficiency: the real parts of the MPTE solutions are the same as calculated for the uncoupled case, while the imaginary parts are the reactances given in (59).
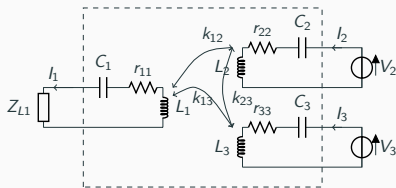
Figure 23: Three–port network showing two transmitters at port 2 and 3 and one receiver at port 1.

In this case, the total power on the loads and the efficiency of the link are given by:

$$
\begin{aligned}
P_{L,TOT} &= P_{L,1} \\
\eta &= \frac{P_{L,1}}{P_{in,1} + P_{in,2}} = \frac{P_{L,1}}{P_{d1} + P_{d2} + P_{d3} + P_{L,1}}
\end{aligned}
\tag{60}
$$

2TX–1RX, Uncoupled receivers (computations)

Assuming that the voltage generators have unit amplitude (i.e., $V_2 = V_3 = 1V$), the following expressions can be derived for the currents:

$$
\begin{aligned}
I_1 &= -j \frac{r_2 x_{13} + r_3 x_{12}}{\Delta} \\
I_2 &= \frac{r_3 R_{L1} + x_{13}^2 - x_{12} x_{13} + r_1 r_3}{\Delta} \\
I_3 &= \frac{r_2 R_{L1} - x_{12} x_{13} + x_{12}^2 + r_1 r_2}{\Delta} .
\end{aligned} \tag{61}
$$

Where the factor Δ has been introduced, which is defined as:

$$
\Delta = r_2 r_3 R_{L1} + r_2 x_{13}^2 + r_3 x_{12}^2 + r_1 r_2 r_3 \tag{62}
$$

By using (61), for the powers dissipated on the resistances $r_i, i = 1, 2, 3$ we get:

$$
\begin{aligned}
P_{d1} &= \frac{1}{2\Delta^2} r_1 \left(r_2 x_{13} + r_3 x_{12} \right)^2 \\
P_{d2} &= \frac{1}{2\Delta^2} r_2 \left(r_3 R_{L1} + x_{13}^2 - x_{12} x_{13} + r_1 r_3 \right)^2 \\
P_{d3} &= \frac{1}{2\Delta^2} r_3 \left(r_2 R_{L1} - x_{12} x_{13} + x_{12}^2 + r_1 r_2 \right)^2
\end{aligned} \tag{63}
$$

similarly, for the power on the load we have:

$$P_{L,1} = \frac{1}{2\Delta^2}(r_2\,x_{13} + r_3\,x_{12})^2\,R_{L1}.\tag{64}$$

By taking the derivative of (64) w.r.t. R_{L1} and equating it to zero, the following value can be obtained for the MPDL load:

$$R_{L1}^p = r_1\theta^2\tag{65}$$

As for the MPTE load, from (63) and (64) the following expression can be derived:

$$R_{L1}^e = r_1\theta\sqrt{1 + \frac{(x_{12} - x_{13})^2}{r_1(r_2 + r_3)}}.\tag{66}$$

This result is different from the result presented in [6]. In particular, by comparing equation (16) of [6] and (66), it can be seen that they are equivalent only in the case $x_{12} = x_{13}$. In fact, according to (66) when $x_{12} = x_{13}$ the expression of R_{L1}^e is simplified as follows:

$$R_{L1}^e = r_1\theta.\tag{67}$$

The Thevenin's equivalent representation of the network with impedance matrix given by (46) can be obtained by considering the open circuit voltage at port one, V_{oc}.

The equivalent impedance can be computed by considering the matrix $Y = Z^{-1}$ in (46) and by taking the element y_{11}. The equivalent impedance seen from port one when the two voltage generators are short–circuited Z_{sc1}, is given by $Z_{sc1} = 1/y_{11}$ or equivalently:

$$Z_{sc1} = r_1 \frac{\theta^2 + \chi_{23}^2}{1 + \chi_{23}^2} - \frac{2 j \, x_{12} \, x_{13} \, x_{23}}{x_{23}^2 + r_2 \, r_3} \tag{68}$$

The optimal impedance $Z_L^p = R_L^p + jX_L^p$ for maximum power transfer is the conjugate of Z_{sc1} and is therefore given by:

$$
\begin{aligned}
R_{L1}^p &= r_1 \frac{\theta^2 + \chi_{23}^2}{1 + \chi_{23}^2} \\
X_{L1}^p &= 2 \, \frac{x_{12} \, x_{13} \, x_{23}}{x_{23}^2 + r_2 \, r_3}
\end{aligned}
\tag{69}
$$

As for the MPTE solution, by considering the equations of the currents, computing the powers and efficiency as in (64), (49) and finding the zero of the derivative w.r.t. to R_L, the following closed form expression can be derived:

$$
\begin{aligned}
a &= \left(r_1 \, x_{13}^2 + 2 \, r_1 \, x_{12} \, x_{13} + r_1 \, x_{12}^2 + r_1^2 \, r_3 + r_1^2 \, r_2 \right) x_{23}^2 \\
b &= r_2 \, x_{13}^4 + \left((r_3 + r_2) \, x_{12}^2 + 2 \, r_1 \, r_2 \, r_3 + r_1 \, r_2^2 \right) x_{13}^2 \\
c &= 2 \, r_2 \, x_{12} \, x_{13}^3 + \left(2 \, r_3 \, x_{12}^3 + 2 \, r_1 \, r_2 \, r_3 \, x_{12} \right) x_{13} \\
d &= r_3 \, x_{12}^4 + \left(r_1 \, r_3^2 + 2 \, r_1 \, r_2 \, r_3 \right) x_{12}^2 + r_1^2 \, r_2 \, r_3^2 + r_1^2 \, r_2^2 \, r_3 \\
e &= (r_3 + r_2) \left(x_{23}^2 + r_2 \, r_3 \right) \\
R_{L1}^e &= \sqrt{\frac{a + b - c + d}{e}} \\
X_{L1}^e &= 0.
\end{aligned}
\tag{70}
$$

It is worth observing that, according to (69)-(70) in the 2TX-1RX configuration with coupled transmitters the MPDL solution is complex (i.e., $X_{L1}^p \neq 0$), whereas the MPTE solution is purely resistive as in the case of uncoupled transmitters.

Table 6: Analytical formulas obtained for the MPDL (columns 2 and 3) and the MPTE solutions (columns 4 and 5) for the 1TX-2RX configuration. It is assumed that a generator is present at port 1, while port 2 and port 3 are terminated on a load $Z_{Li} = R_{Li} + jX_{Li}$, $i = 1, 2$.

Parameter	uncoup. RX MPDL	coup. RX MPDL	uncoup. RX MPTE	coup. RX MPTE
R_{L2}	$r_2\theta^2$	$=$	$r_2\theta$	$=$
R_{L3}	$r_3\theta^2$	$=$	$r_3\theta$	$=$
X_{L2}	0	$-\frac{r_2\,x_{13}\,x_{23}}{r_3\,x_{12}}$	0	$-\frac{r_2\,x_{13}\,x_{23}}{r_3\,x_{12}}$
X_{L3}	0	$-\frac{r_3\,x_{12}\,x_{23}}{r_2\,x_{13}}$	0	$-\frac{r_3\,x_{12}\,x_{23}}{r_2\,x_{13}}$

Table 7: Analytical formulas obtained for the MPDL solution.

Parameter	uncoup. TX	coup. TX
R_{L1}	$r_1 \theta^2$	$r_1 \dfrac{\theta^2 + \chi_{23}^2}{1 + \chi_{23}^2}$
X_{L1}	0	$2 \dfrac{x_{12}\, x_{13}\, x_{23}}{x_{23}^2 + r_2\, r_3}$

Table 8: As in the previous table but for the MPTE solution.

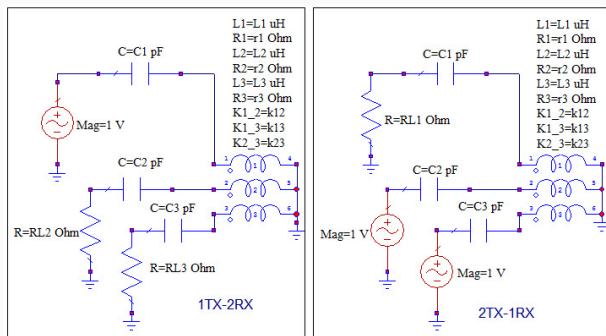| Parameter	uncoup. RX	coup. RX
R_{L1}	$r_1 \theta \sqrt{1 + \dfrac{(x_{12} - x_{13})^2}{r_1(r_2 + r_3)}}$	$\sqrt{\dfrac{a + b - c + d}{e}}$
X_{L1}	0	0

Figure 24: Schematic of the circuits analyzed by circuit simulations for the 1Tx-2RX configuration (on the left) and the 2TX-1RX configuration (on the right).

Analyzed configuration 2

Table 9: WPT link consisting of three coupled resonators. Three different cases are considered: the case where resonator 1 is equally coupled with resonators 2 and 3, while resonators 2 and 3 are uncoupled (case A); the case where resonator 1 is differently coupled with resonators 2 and 3, while resonators 2 and 3 are uncoupled (case B); the case where all the resonators are coupled and all the mutual couplings are different (case C).

Parameter	case A	case B	case C
f_0	6.78 MHz	=	=
$L_1 = L_2 = L_3$	4.59 µH	=	=
$C_1 = C_2 = C_3$	120 pF	=	=
$Q_1 = Q_2 = Q_3$	270	=	=
k_{12}	0.15	=	=
k_{13}	0.15	0.1	=
k_{23}	0.00	=	0.09

Table 10: Results obtained by circuit simulations for the 1TX-2RX configuration of the three coupled resonators described in Table 9. We have assumed that a 1 V generator is present at port 1, while port 2 and port 3 are terminated on a load $Z_{Li} = R_{Li} + jX_{Li}$, $i = 1, 2$. The results for case C have been calculated by adding two series compensating capacitances to R_{L2} and R_{L3}. The powers are in mW and the resistances are in Ω.

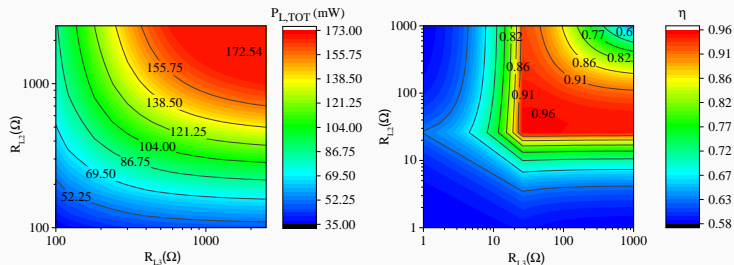| Parameter	MPDL case B	MPDL case C	MPTE case B	MPTE case C
R_{L2}	1716.5	=	35.25	=
R_{L3}	1716.5	=	35.25	=
X_{L2}	0	-11.73	0	-11.73
X_{L3}	0	-26.4	0	-26.4
P_{d1}	172.75	=	0.29	=
P_{d2}	0.05	=	0.19	=
P_{d3}	0.022	=	0.09	=
P_{L2}	119.45	=	9.42	=
P_{L3}	53.09	=	4.19	=
$P_{L,TOT}$	172.53	=	13.61	=
η	0.50	=	0.96	=

Figure 25: Results obtained by circuit simulations for the 1TX-2RX configuration: total power and efficiency behavior for case B.

As for case C, as it can be seen from Table 10, circuit simulations confirm that the use of the compensating reactances X_{Li}, corresponding to two series capacitances ($C_{c2} = 2\,\mathrm{nF}$, $C_{c3} = 0.889\,\mathrm{nF}$), allows retrieving the same results obtained for the uncoupled case (i.e., case B).

Configuration 2TX-1RX

Table 11: Results calculated by circuit simulations for the 2TX-1RX configuration: maximum power case. The element values are listed in Table 9; we have assumed that a 1 V generator is present at port 1 and at port 2. The powers are in mW and the resistances are in Ω.

Parameter	case A	case B	case C
R_{L1}	2375.8	1716.5	3.6
X_{L1}	0	0	65.068
P_{d1}	0.11	0.14	53.43
P_{d2}	172.66	123.72	66.08
P_{d3}	172.66	261.59	148.48
P_{L1}	345.12	331.8	265.61
η	0.5	0.46	0.5

Configuration 2TX-1RX

Table 12: Results calculated by circuit simulations for the 2TX-1RX configuration: maximum efficiency case. We have assumed that a $1\,\text{V}$ generator is present at port 1 and at port 2. The powers are in mW and the resistances are in Ω.

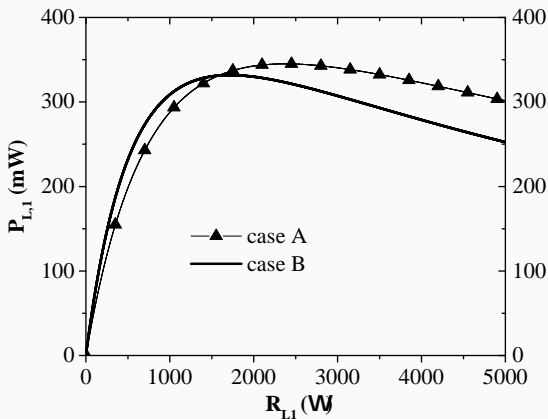| Parameter	case A	case B	case C
R_{L1}	41.5	338.4	37.2
X_{L1}	0	0	0
P_{d1}	0.4	0.39	0.47
P_{d2}	0.21	0.92	0.30
P_{d3}	0.21	88.34	0.35
P_{L1}	23.29	182.57	24.28
η	0.97	0.67	0.96

Figure 26: Results obtained for the 2TX-1RX configuration: power on the load calculated by circuit simulations for case A and B.
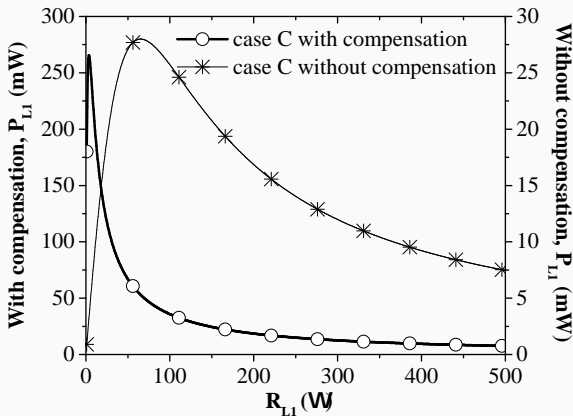
Figure 27: Results calculated for the 2TX-1RX configuration. Power on the load calculated by circuit simulations for case C: results obtained with and without the compensating reactance X_{L1}.
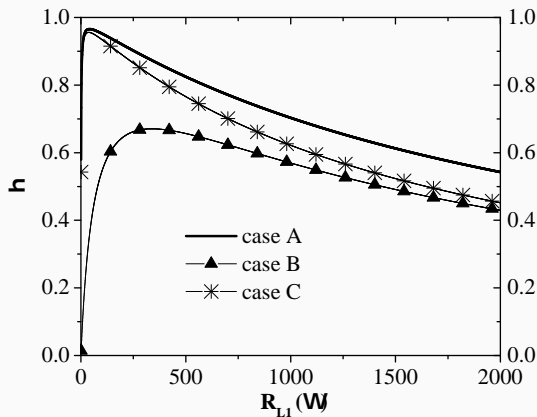
Figure 28: Results calculated for the 2TX-1RX configuration: results obtained by circuit simulations for the efficiency.

Conclusions for three–ports

Two different configurations have been examined, solved and validated in all cases.

For the 1TX–2RX configuration, it has been demonstrated that the loads that maximize both the efficiency and the power are purely resistive; whereas, reactive compensating elements are necessary when the receivers are coupled. More specifically, it has been shown that the solutions for the coupled case are the same as the uncoupled case except for the necessity of adding appropriate compensating reactances.

For the 2TX–1RX configuration, the load that realizes the MPTE condition is purely resistive for both the case of uncoupled and coupled transmitters. Conversely, the load that realize MPDL is purely resistive in the case where the transmitters are uncoupled, while it is complex in the case of coupled transmitters. In the case coupled TX use of the compensating reactances allows to retrieve about 10 times more power!

H. Baudrand.
On the generalizations of the maximum power transfer theorem.
Proceedings of the IEEE, 58(10):1780–1781, 1970.

T. S. Bird, N. Rypkema, and K. W. Smart.
Antenna impedance matching for maximum power transfer in wireless sensor networks.
IEEE Sensors, pages 916–919, 2009.

B. L. Cannon, J. F. Hoburg, D. D. Stancil, and S. C. Goldstein.
Magnetic Resonant Coupling As a Potential Means for Wireless Power Transfer to Multiple Small Receivers.
IEEE Transactions on Power Electronics, 24(7):1819–1825, Oct. 2009.

References II

M. Dionigi, M. Mongiardo, and R. Perfetti.
Rigorous network and full-wave electromagnetic modeling of wireless power transfer links.
Microwave Theory and Techniques, IEEE Transactions on, 63(1):65–75, Jan 2015.

M. Fu, T. Zhang, C. Ma, and X. Zhu.
Efficiency and optimal loads analysis for multiple-receiver wireless power transfer systems.
IEEE Transactions on Microwave Theory and Techniques, 63(3):801–812, Mar 2015.

K. Lee and D. Cho.
Diversity Analysis of Multiple Transmitters in Wireless Power Transfer System.
IEEE Transactions on Magnetics, 49(6):2946–2952, 2013.

📄 M. Mongiardo, Q. Wang, W. Che, M. Dionigi, R. Perfetti, Y. Chang, and G. Monti.
Wireless Power Transfer Between One Transmitter and Two Receivers: Optimal Analytical Solution.
In *Asia-Pacific Microwave Conference*, 2015.

📄 F. Spinei.
On generalizations of the maximum power transfer problem.
Proceedings of the IEEE, 60(7):903–904, 1972.

📄 M. Zargham and P. G. Gulak.
Maximum Achievable Efficiency in Near-Field Coupled Power-Transfer Systems.
IEEE Transactions on Biomedical Circuits and Systems, 6(3):228–245, 2011.